Excitation of Langmuir Wave Turbulence by High-Frequency (HF) Pump Waves Over Gakona, Alaska

by

Daniel L. Rokusek

B.S. Nuclear Engineering
University of Illinois at Urbana-Champaign, 2005

SUBMITTED TO THE DEPARTMENT OF NUCLEAR SCIENCE AND ENGINEERING IN PARTIAL FULFILLMENT OF THE REQUIREMENTS FOR THE DEGREE OF

MASTER OF SCIENCE IN NUCLEAR ENGINEERING
AT THE
MASSACHUSETTS INSTITUTE OF TECHNOLOGY

FEBRUARY 2007

Signature of Author: _____
Department of Nuclear Science and Engineering
December 19, 2006

Certified by: _____
Prof. Min-Chang Lee
Leader of Ionospheric Plasma Research Group
Thesis Supervisor

Certified by: _____
Prof. Jeffrey P. Freidberg
Professor of Nuclear Science and Engineering
Thesis Reader

Certified by: _____
Prof. Jeffrey A. Coderre
Associate Professor of Nuclear Science and Engineering
Chairman, Committee for Graduate Students

Excitation of Langmuir Wave Turbulence by High-Frequency (HF) Pump Waves Over Gakona, Alaska

by

Daniel L. Rokusek

Submitted to the Department of Nuclear Science and Engineering
on December 19, 2006 in Partial Fulfillment of the
Requirements for the Degree of Master of Science in
Nuclear Engineering

ABSTRACT

Investigated in this thesis are the excitation and observation of Langmuir wave turbulence caused by the parametric decay instability (PDI) in high-frequency space plasma heating experiments conducted at the NSF/DoD High Frequency Active Auroral Research Program (HAARP) facility in Gakona, Alaska during the spring and summer of 2006. The PDI is the decay of an electromagnetic (EM) wave into an electron plasma wave (i.e., Langmuir wave) and an ion acoustic wave. When the excited Langmuir wave parametrically decays into another Langmuir and ion acoustic wave pair, a cascade of Langmuir waves can occur provided that the instability threshold is satisfied. According to recently advanced theory by Kuo and Lee [2005], there are two possible methods of cascade: non-resonant and resonant. While the non-resonant cascade proceeds at the location of excitation, the resonant process occurs at lower altitudes to minimize losses that the non-resonant process incurs by remaining at the excitation altitude. Such losses are caused by the frequency mismatch effect, as the decay ion acoustic wave frequency becomes much less than that of the normal ion acoustic waves. In their downward propagation the Langmuir waves in the resonant cascade suffer from propagation losses, however these losses are less than those associated with the non-resonant process. The resonant process is therefore expected to have a lower threshold. Theoretical claims and calculations are compared to observations made at Arecibo, Puerto Rico and Tromso, Norway. Claims are also are supported by incoherent backscatter radar observations made at the HAARP facility in Gakona.

Thesis Supervisor: Prof. Min-Chang Lee
Title: Leader of Ionospheric Plasma Research Group

Acknowledgements

I would like to express sincere gratitude and the utmost respect for Professor Min-Chang Lee for the guidance and support he has given me. From his tutorial lectures in the beginning of my studies of ionospheric plasma physics to the conceptual discussions that led to the completion of this thesis, he has always made himself available for anything that I need. I have learned a great deal about plasma physics and its applications in the three semesters I have spent as his student and have gained invaluable experience pertaining to the experimental campaigns at prestigious facilities in Gakona (for this thesis) and Arecibo (for other work not pertaining to this thesis). The realm of the knowledge he has bestowed upon me is not limited to academia, as I take with me important life lessons. I admire his dedication to teaching and aspire to develop many of the qualities he possesses. I thank Professor Lee for helping me through a cross roads in my academic career, and finally for all of the time and patience he has given to me and put towards the completion of this thesis.

I would also like to express many thanks to Professor Jeffrey Freidberg for serving as my thesis reader. Before he agreed to be the reader of this thesis, Professor Freidberg was my academic advisor and instructor for two courses. In both roles he was available to me whenever I needed something. His love of teaching is obvious to anyone that sits in his classroom and is an inspiration to an aspiring young scientist with hopes of a future in education.

Finally I would like to thank my peers and fellow students in the Ionospheric Plasma Research Group at the MIT Plasma Science and Fusion Center for all of their efforts and assistance. Each of them welcomed me into the group and contributed to a friendly environment around the lab. I especially thank Rezy Pradipta for everything he has done for me. From teaching me about data analysis techniques to answering all of my conceptual questions, Rezy has impressed me with his knowledge, dedication, and hard work.

Financial support for this work came from the Air Force Office of Scientific Research. I thank them for their generous support.

Contents

List of Figures

List of Tables

Chapter 1

Introduction

1.1 Background and Context

Langmuir wave turbulence has been observed as a result of high-frequency (HF) ionospheric heating experiments. Some turbulence caused by HF O-mode pump waves can be characterized by the detection of cascading Langmuir waves by backscatter radars. Based on recently advanced theory, such turbulence is believed to be produced via the parametric decay instability (PDI) [*Lee et al.*, 1997 and references therein]. This thesis will focus on the results of HF space plasma heating experiments conducted at the NSF/DoD High Frequency Active Auroral Research Program (HAARP) facility in Gakona, Alaska during the spring and summer of 2006. In doing so, the PDI process will be explained; advanced theory of Kuo and Lee [2005] will be examined; and experimental results will be discussed, interpreted, and compared to the theory of Kuo and Lee.

The PDI is a three-wave interaction process involving an electromagnetic (EM) wave, an electron plasma wave (i.e., Langmuir wave), and an ion acoustic wave. When sufficient energy is provided to overcome the instability threshold, the EM wave decays into the electron plasma wave and ion acoustic wave. The daughter Langmuir wave can then decay into another pair of Langmuir wave and ion acoustic wave, creating a cascade of Langmuir and ion acoustic waves. Excitation energy can be provided by natural or man-made sources. One such man-made source is in the form of injected HF electromagnetic waves from an antenna array at the HAARP facility in Gakona. A backscatter radar is used to detect and measure the excited waves. It is important to note

that the radar can only detect Langmuir waves that propagate parallel or antiparallel to the radar and have a wave number equal to twice the wave number of the radar. Such waves are called "HF wave enhanced plasma lines" (HFPLs). Detected HFPLs propagating downward towards the radar are said to be down-going and are referred to as frequency upshifted Langmuir waves, while HFPLs propagating away from the radar are up-going and called frequency downshifted Langmuir waves.

As stated above, energy must be provided to excite the PDI. The source of this energy is a ground-based HF heater operating in pulsed O-mode. The process leading up to the excitation of the PDI involves the injection of RF waves from the heater and their conversion to O-mode plasma waves in the ionosphere. When the converted O-mode waves near their reflection height, their group velocity decreases. Conservation of flux dictates that a decrease in group velocity must be compensated by an increase in energy, therefore a swelling in energy occurs near the reflection height. It is this swelling effect that meets and exceeds the threshold energy of the PDI, thereby triggering the instability. The cartoon provided in figure 1-1 illustrates the swelling in electron density. The O-mode pump wave decays into a Langmuir wave and an ion acoustic wave. A cascade of Langmuir and ion acoustic waves occurs, as the daughter Langmuir wave decays into a granddaughter Langmuir wave and a second ion acoustic wave. Thus, a Langmuir sideband is created.

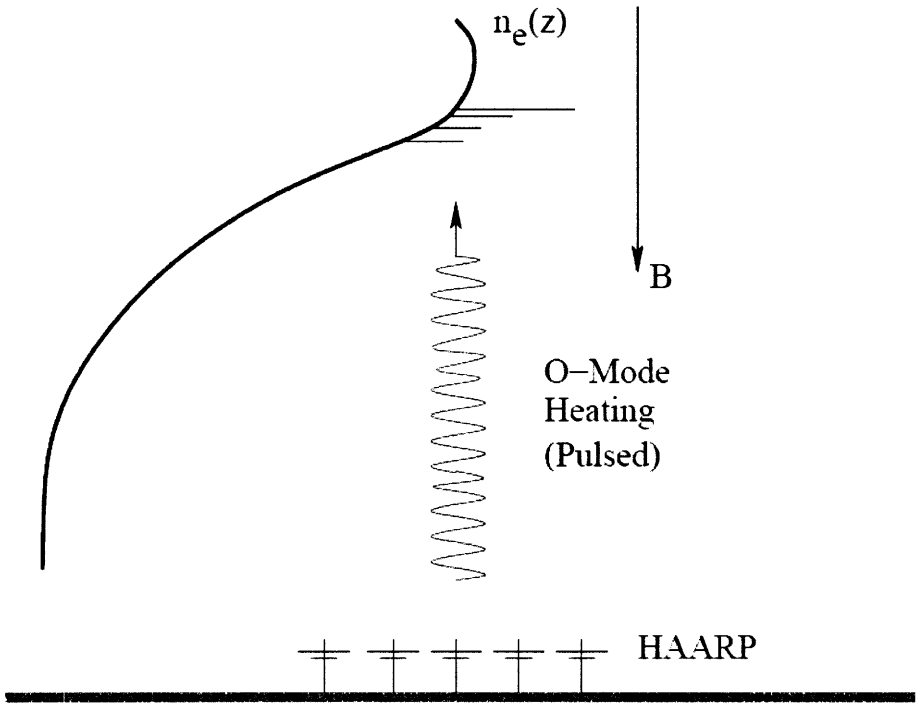

Figure 1-1: This cartoon is a generalization of the swelling effect observed at Gakona, where the earth's magnetic field is exaggerated as being vertical [*Pradipta*, 2006].

The phenomenon observed near the reflection height of the O-mode plasma wave that triggers the PDI can be compared to the phenomenon observed in tsunami waves [*Lee et al.*, 2006]. Tsunami waves are water waves characterized by having relatively small amplitudes offshore and large wavelengths. As the tsunami waves move towards land, the depth of the water below the surface decreases. This decrease in depth causes the tsunami's group velocity to decrease, and the wave seemingly piles up on itself. When the wave makes landfall, the group velocity is small such that the wave has much more energy than it did offshore, and the effects are catastrophic. Conservation of flux can again be used to describe this behavior, where we observe a dramatic increase in energy corresponding to the decrease in group velocity.

Kuo and Lee [2005] have established a theory of the cascade spectra of Langmuir waves from electromagnetic wave-excited PDI. In this case, the electromagnetic wave is a HF O-mode pump wave, and it produces a Langmuir wave and an ion acoustic wave. The excited Langmuir wave then becomes a parent pump wave to excite the next generation of Langmuir and ion acoustic waves. This process will repeat until the

instability is saturated or until the n^{th} generation Langmuir wave cannot achieve the PDI threshold.

Kuo and Lee's theory predicts both resonant and non-resonant cascade processes. The notable differences between the two processes involve instability threshold, losses, and altitude of PDI. The resonant cascade process has a lower threshold and is expected to occur at lower altitudes to minimize losses from the frequency mismatch effect. The subsequent propagation losses govern the number of generations that can satisfy the decay thresholds. In contrast, the non-resonant cascade process will occur near the reflection height of the O-mode pump wave with much greater thresholds. The reason is that PDI will suffer from the frequency mismatch effect, as the decay ion acoustic wave frequency becomes much less than that of the normal ion acoustic waves. These behaviors are expected in this case because ion Landau damping will play a significant role in imposing a higher threshold of the PDI [*Kuo and Lee*, 2005].

1.2 Hypothesis

It is predicted that the propagation losses associated with the resonant cascade process will be less than the losses from the frequency mismatch effect for the non-resonant process. It is therefore expected that the radar will detect a downward step in altitude of the Langmuir wave in each subsequent generation of the cascade. To verify this, values for the propagation loss in the resonant process and for the frequency mismatch effect in the non-resonant process will be presented. The plot in figure 1-2 illustrates the detection of a downward step in altitude for four generations in a resonant cascade process. The figure contains the expected cascade spectra to be observed at HAARP.

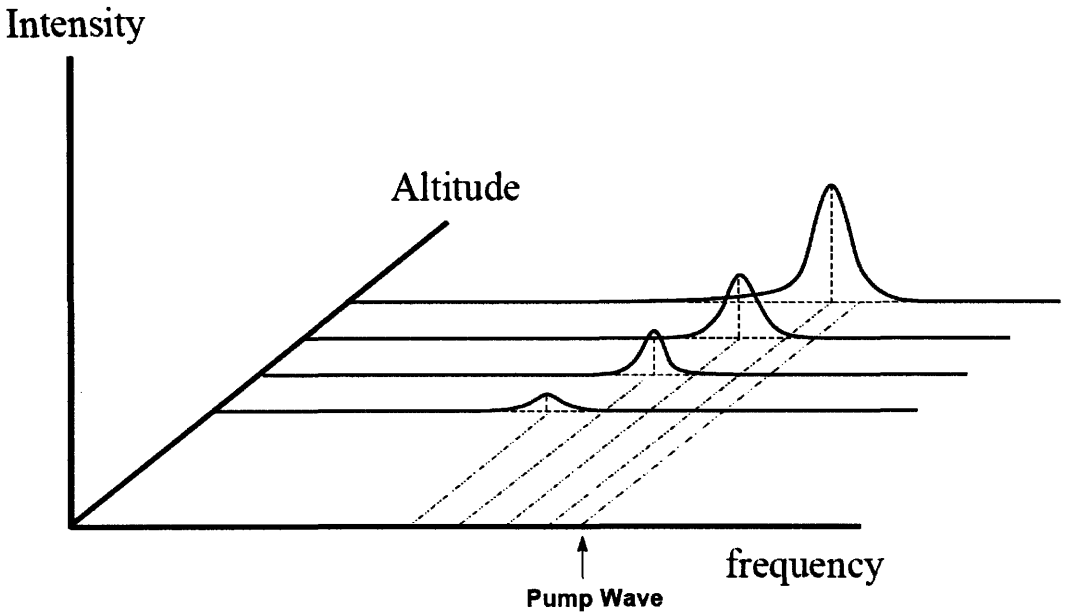

Figure 1-2: An illustration of the expected cascade spectra in a resonant process [*Pradipta*, 2006].

1.3 Motivation

This work was motivated by similar heating experiments that were conducted over Arecibo, Puerto Rico and Tromso, Norway [*Kuo and Lee*, 2005]. The theory behind the previously conducted experiments will be applied to the experiments conducted over Gakona. When this theory was first presented, radar diagnostics were not powerful enough to properly test the theory. The HAARP facility now has the ability to offer the necessary diagnostics to test the theory. Verification of the theory is important, as it can lead to further advancement of the field of non-linear plasma physics, as well as a better understanding of the PDI and its applications. The geographical location of the HAARP facility is unique, offering the chance to perform experiments where the earth's magnetic field lines are nearly vertical. Such experiments will contrast those conducted in Arecibo, where the earth's magnetic field lines are about 50 degrees with respect to the horizon. Another motivating factor for this work was the opportunity to explore and characterize

the capabilities of newly constructed Modulated UHF Ionosphere Radar (MUIR) at the HAARP facility.

In general, studies of the PDI can lead to advancements in non-linear plasma physics when applied to plasma heating. The PDI process is one that produces Langmuir waves, and it is known that Langmuir waves can heat electrons and then ions. The ability to effectively and efficiently heat a plasma is important in a variety of plasma physics experiments. Space heating experiments are particularly attractive because they offer a unique opportunity to study the PDI in a stable environment. It is this stability of the ionospheric plasma and also the reproducibility of results that make space heating experiments useful. Understanding the PDI is also important in the field of laser fusion, where similar instabilities are observed. However, because the pellet used in such experiments as well as the time scale of the reaction are so small, studies of the PDI in laser fusion experiments have proven to be challenging as diagnostic equipment cannot successfully identify and characterize PDI events. Thus, heating experiments performed in space are preferred.

1.4 Comments on Experiments

Experiments at the HAARP facility in the spring and summer of 2006 were conducted with the HF heater tilted along the magnetic zenith, operating in a pulsed O-mode. The pump waves generated by the HAARP HF heater served as the source to excite the PDI. In the summer, the heater pulse was a 10-second cycle, with the heater on for 2 seconds and off for 8 seconds. As mentioned above, HAARP is an ideal location for these experiments because the magnetic zenith is nearly vertical at Gakona's high latitude. This experimental setup offers an opportunity to study the physics when the magnetic field lines and wave propagation are anti-parallel. Previous experiments have been performed with oblique propagation, where magnetic field lines have a dip angle of ~50 degrees. Having the ability to operate the heater anti-parallel to the earth's magnetic field lines improved the chances of excitation of the PDI. The parallel propagation of the O-mode

heater waves simulated the propagation of waves in unmagnetized plasma. This simplifies the dispersion relation and improves coupling. Tilting MUIR along the earth's magnetic field lines was essential also because the only detectable HFPLs are those parallel or anti-parallel to the radar. Thus, the chances of detecting PDI excited Langmuir waves were maximized with this particular geometry.

Results from the experiments performed in the spring and summer of 2006 showed a cascade of upshifted Langmuir waves. These results were diagnosed and recorded using the newly constructed MUIR incoherent scatter radar. The detected HFPLs were excited Langmuir waves whose wave numbers were equal to twice that of the MUIR signal. Because the resonant process is predicted to be the method at which the HFPLs cascade, altitude of each cascade step was sought and spatial resolution of the radar was maximized. There is an inverse relationship between spatial and frequency resolution in radars, thus the frequency resolution of the recorded data during the spring 2006 experiments was of lower quality. Due to the restrictions of the summer 2006 experimental campaign, frequency resolution was maximized causing spatial resolution to suffer. Therefore the presented data from the summer of 2006 does not offer as much insight to the step down in altitude of the steps in the decay cascade. In other words, after analysis, the results from the two experimental campaigns did not conclusively detect a decrease in altitude in the cascade of Langmuir waves. Fortunately, we have an additional set of data acquired from an earlier campaign to offer evidence that supports the theoretical claims of the resonant process, and therefore the excited instabilities are said to cascade via the resonant cascade process.

Presented in chapter 2 will be the theoretical basis for this work. Chapter 3 will feature theoretical calculations and discussion of said calculations. Experimental results will be given in chapter 4, along with appropriate discussion. Finally, conclusions will be drawn in chapter 5. Appendix A is provided to support the discussion of experimental data in chapter 4.

Chapter 2

Theoretical Basis

A cascade of Langmuir waves will arise as a result of two decay events. The first decay event is of an O-mode pump wave into a Langmuir wave and an ion acoustic wave. The O-mode waves are the converted radio waves injected by the HF heater at HAARP. This decay occurs via the PDI, triggered near the reflection height of the O-mode wave due to the swelling effect. The second decay event is of the produced Langmuir wave into another pair of Langmuir wave and ion acoustic wave. This creates a sideband of frequency-downshifted Langmuir waves, as generations of parametric instabilities are excited.

The dispersion relations for the O-mode pump wave, Langmuir wave, and ion acoustic waves are, respectively: $\omega_o^2 = \omega_{pe}^2 + k_o^2c^2$, $\omega_L^2 = \omega_{pe}^2(1 + 3k_l\lambda_{De}^2) = \omega_{pe}^2 + 3k_lv_{te}^2$, and $\omega_{IA}^2 = C_s^2k_{IA}^2$. Figures 2-1 and 2-2 below illustrate parallelogram constructions of the two decays discussed above, namely the decay of the O-mode pump wave into the mother Langmuir wave and ion acoustic wave and the decay of the mother Langmuir wave into the daughter Langmuir wave and ion acoustic wave.

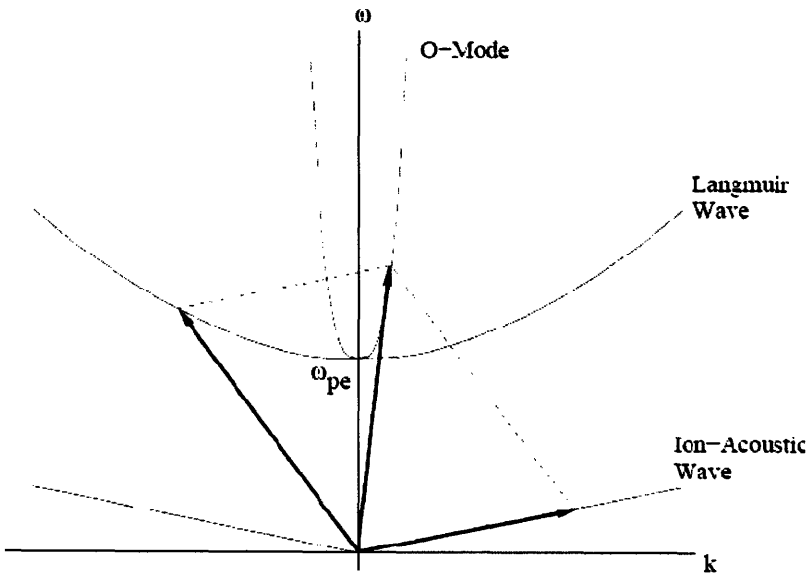

Figure 2-1: Decay of O-mode pump wave into Langmuir and ion acoustic waves [*Pradipta*, 2006].

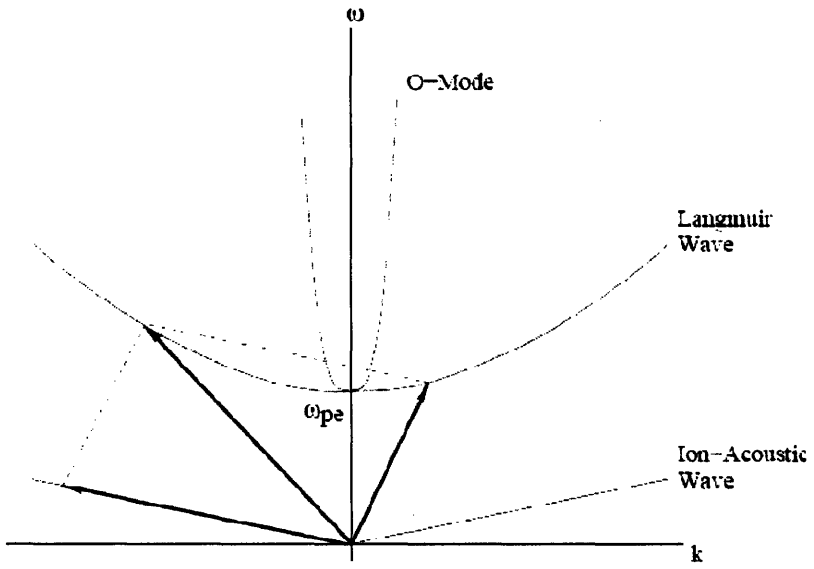

Figure 2-2: Decay of mother Langmuir wave into daughter Langmuir and ion acoustic waves [*Pradipta*, 2006].

Frequency and wave vector matching relations can be taken from the figures above. From figure 2-1 we have $\omega_o = \omega_L + \omega_{IA}$ and $\mathbf{k}_o = \mathbf{k}_L + \mathbf{k}_{IA}$, and from figure 2-2 we have $\omega_L = \omega_{L'} + \omega_{IA'}$ and $\mathbf{k}_L = \mathbf{k}_{L'} + \mathbf{k}_{IA'}$. Since $|\mathbf{k}_o| \ll 1$, we can take $|\mathbf{k}_L| \approx -|\mathbf{k}_{IA}|$ and find

that $\mathbf{k}_{IA'} \approx -2\mathbf{k}_{IA}$. Now that the decay processes have been defined, the necessary theory will be discussed.

The theoretical basis for this thesis is drawn from theory established by Kuo and Lee [2005]. They proposed that the decay of a Langmuir wave into a Langmuir sideband and an ion acoustic wave can occur via the PDI; and experiments conducted in Arecibo, Puerto Rico and Tromso, Norway supported the theory. Cascades of Langmuir waves were observed to occur in resonant and non-resonant decay processes. Because the experiments conducted for this work are similar to those conducted in Puerto Rico and Norway, Kuo and Lee's theory is applied here with confidence. The goal for applying Kuo and Lee's theory in this thesis is to determine theoretical values for characteristic quantities for comparison with experimental data from the 2006 Gakona experimental campaigns. Quantities of particular interest are the instability thresholds and loss terms. Comparison of the theoretical instability thresholds and individual loss terms will suggest the preferred cascade process, be it resonant or non-resonant. It is known that the resonant cascade process's threshold is less than that of the non-resonant cascade process, and it is predicted that the losses caused by downward propagation in the resonant cascade process are less than the losses from ion Landau damping in the non-resonant cascade process. These claims will now be investigated using the reputable theory.

2.1 Coupled Mode Equations

Analysis begins with a change of notation. First, let the mother Langmuir wave be represented by $\phi_1(\omega_1,\mathbf{k}_1)$, formerly $\phi_L(\omega_L,\mathbf{k}_L)$. Second, let the Langmuir sideband be represented as $\phi_2(\omega_2,\mathbf{k}_2)$, formerly $\phi_{L'}(\omega_{L'},\mathbf{k}_{L'})$. Finally, let the ion acoustic wave be represented as $n_{s1}(\omega_{s1},\mathbf{k}_{s1})$, formerly $n_{IA}(\omega_{IA},\mathbf{k}_{IA})$ and $n_{IA'}(\omega_{IA'},\mathbf{k}_{IA'})$. With these changes in notation, note that the relationships between wave vectors are now $\mathbf{k}_2 \approx -\mathbf{k}_1$ and $\mathbf{k}_{s1} \approx 2\mathbf{k}_1$.

Now, proceed by deriving the coupled mode equations. For the Langmuir sideband, the coupled mode equation is derived by combining the electron continuity and momentum equations with Poisson's equation:

$$\begin{aligned}&\left\{\left[\left(\partial_t+\nu_e\right)^2+\Omega_e^2\right]\left(\partial_t^2+\nu_e\partial_t+\omega_p^2-3v_{te}^2\nabla^2\right)\nabla^2-\Omega_e^2\left(\omega_p^2-3v_{te}^2\nabla^2\right)\nabla_\perp^2\right\}\phi_2 \\ &=-\omega_p^2\left\{\left[\left(\partial_t+\nu_e\right)^2\nabla+\Omega_e^2\nabla_z\right]\cdot\left\langle\nabla\phi_1\left(n_{s1}^*/n_0\right)\right\rangle-\Omega_e\left(\partial_t+\nu_e\right)\cdot\left\langle\nabla\left(n_{s1}^*/n_0\right)\times\nabla\phi_1\right\rangle\right\},\end{aligned} \tag{2.1}$$

where $\omega_p^2 = (4\pi n_0 e^2 / m_e)$ is the electron plasma frequency; $\langle\ \rangle$ represents a filter that rejects terms not having the same phase function as that of the function on the left hand side of the equation; $\nu_e = \nu_{ei} + \nu_{eL}$, ν_{ei} is the electron-ion collision frequency and $\nu_{eL} = (\pi/2)^{1/2}(\omega_0^2\omega_p^2 / k_z k^2 v_{te}^3)\exp(-\omega_0^2 / 2k_z^2 v_{te}^2)$ is the electron Landau damping rate, which accounts for the lowest-order kinetic effect.

The coupled fluid equations of electrons and ions can be used to derive the coupled mode equation for the low-frequency decay mode. The result is:

$$\begin{aligned}&\left\{\left[\nabla_\perp^2\partial_t\left(\partial_t+\nu_e\right)+\Omega_e^2\nabla_z^2\right]\left[\partial_t\left(\partial_t+\nu_i\right)-C_s^2\nabla^2\right]+\Omega_e\Omega_i\nabla_\perp^2\partial_t^2\right\}\cdot\left(n_{s1}/n_0\right) \\ &=\left(m/M\right)\nabla^2\left[\left(\partial_t+\nu_e\right)\partial_t\nabla_\perp\cdot\mathbf{a}_p+\Omega_e^2\partial_z a_{pz}-\Omega_e^2\partial_t\nabla\cdot\mathbf{J}_B/n_0-\Omega_e\partial_t\nabla\cdot\mathbf{a}_p\times\hat{\mathbf{z}}\right],\end{aligned} \tag{2.2}$$

where $\mathbf{a}_p = \langle \mathbf{v}_e \cdot \nabla \mathbf{v}_e \rangle$ and $\mathbf{J}_B = \langle n_e \mathbf{v}_e \rangle$; $\Omega_i^2 \ll |\partial_t^2|$ and $|\Omega_i^2 \nabla_z^2| \ll |\partial_t^2 \nabla_\perp^2|$ are assumed; $\nu_e = \nu_{ei}$ and $\nu_i = \nu_{in} + \nu_{iL}$, ν_{in} is the ion-neutral particle collision frequency and $\nu_{iL} \cong (\pi/2)^{1/2}(\omega_s^2 / k_z k v_{ti})(T_e / T_i)\exp(-\omega_s^2 / 2k_z^2 v_{ti}^2)$ is the ion Landau damping rate.

The instability dispersion relation can be derived from equations 2.1 and 2.2. When the geometry is such that $\mathbf{k}_1 = \mathbf{k}_0 + \mathbf{k}_\perp$ and $\mathbf{k}_2 = -\mathbf{k}_1$, in the x-z plane, and $\mathbf{k}_{s1} = 2\mathbf{k}_1$, the dispersion relation is found to be:

$$\begin{aligned}&\left[\omega_2\left(\omega_2+\mathrm{i}\nu_e\right)-\omega_{k\theta}^2\right]\left[\omega_{s1}^*\left(\omega_{s1}^*-\mathrm{i}\nu_i\right)-4k_1^2C_s^2\right] \\ &=k_1^2\left[k_0^2+k_\perp^2\omega_1^2/\left(\omega_1^2-\Omega_e^2\right)\right]\left(\omega_p^4/\pi n_0 M\omega^2\right)\left|\phi_1\right|^2,\end{aligned} \tag{2.3}$$

where $\omega_{k\theta}^2 = \omega_p^2 + 3k_1^2 v_{te}^2$; and $|\Omega_e^2 \nabla_e^2| \gg |\partial_t(\partial_t + \nu_e)\nabla_\perp^2|$ and $|\Omega_e \Omega_i \nabla_\perp^2|$ are assumed for the coupled mode equation for the low-frequency decay mode. With this dispersion

relation, the excitation of the Langmuir sideband's first cascade line from PDI can be analyzed. It is at this point that the resonant and non-resonant decay processes are treated differently. Different treatment is needed because the two cascade processes occur at different altitudes. The non-resonant decay process creates a forced mode at the same altitude of the PDI, and coupling is reduced causing the instability threshold to be larger in order to account for the fact that the Langmuir wave's dispersion relation is not satisfied at the altitude of PDI. While the non-resonant decay occurs at the same altitude as that of the PDI, the resonant decay occurs at a lower altitude than that of the PDI. This downward propagation is necessary for the resonant process because the Langmuir sideband is not a local plasma mode of the parametric instability at the altitude of the PDI. Consequently, each cascade step occurs at increasingly lower altitudes, and it is important to include the propagation loss the Langmuir waves experience when calculating the instability's threshold.

2.2 Non-Resonant Cascade Process

To obtain the threshold field for the non-resonant decay process, the instability growth rate γ is introduced by breaking down the frequencies into their real and imaginary parts. With $\omega_{k\omega} = \omega_1$ (since the process occurs at the height of the PDI), the wave frequencies become: $\omega_{s1} = \omega_{s1r} + i\gamma$ and $\omega_2 = \omega_{k\theta} - \omega_{s1r} + i\gamma$. When these frequencies are inserted into the instability dispersion relation, real and imaginary terms can be grouped to produce two real equations:

$$(2\gamma+\nu_e)\left[4k_1^2C_s^2+\gamma(\gamma+\nu_i)-\omega_{s1r}^2\right]=2\omega_{s1r}^2(2\gamma+\nu_i) \tag{2.4}$$

and

$$\begin{aligned}&2\omega_{k\theta}\omega_{s1r}\left[4k_1^2C_s^2+\gamma(\gamma+\nu_i)-\omega_{s1r}^2\right]+\omega_{k\theta}\omega_{s1r}(2\gamma+\nu_e)(2\gamma+\nu_i)\\&=k_1^2\left[k_0^2+k_\perp^2\omega_{k\theta}^2/\left(\omega_{k\theta}^2-\Omega_e^2\right)\right]\left(\omega_p^4/\pi n_0 M\omega_{k\theta}^2\right)|\phi_1|^2.\end{aligned} \tag{2.5}$$

The threshold field will occur when $\gamma = 0$. Before this threshold can be obtained, the decay mode frequency must first be found. By letting $\gamma = 0$, equation 2.4 is reduced to $\omega_{s1r}^2 = [\nu_e / (\nu_e + 2\nu_i)]4k_1^2C_s^2$, the decay mode frequency. Inserting this result into equation 2.5 and reducing will give the condition for the instability threshold:

$$|\phi_1|_{th}^2 = G_1|\phi|_0^2 = G_1|E_{pth}(k,\theta)|^2 \cos^2\theta / 2\left[k_0^2 + k_\perp^2\omega_0^2 / (\omega_0^2 - \Omega_e^2)\right], \qquad (2.6)$$

where $|\phi|_0^2 = (mM/e^2)\{k_1C_s\omega_{k\theta}^3\nu_e\nu_i / 2k_1^2[k_0^2 + k_\perp^2\omega_{k\theta}^2 / (\omega_{k\theta}^2 - \Omega_e^2)]\ \omega_p^2\} \cong |E_{pth}(k, \theta)|^2 \cos^2\theta/2\ [k_0^2+k_\perp^2\omega_0^2 / (\omega_0^2 - \Omega_e^2)]$ is the threshold condition for the first resonant cascade, $|E_{pth}(k, \theta)|^2$ is the field amplitude of PDI; k and θ are the wave number and oblique propagation angle of the Langmuir sideband of PDI; $G_1 = [1+16k_1^2C_s^2/\nu_e(\nu_e+2\nu_i)]\ [\nu_e/(\nu_e+2\nu_i)]^{1/2}$.

The threshold for the first cascade line of the non-resonant decay cascade process can be calculated using equation 2.6. To calculate the threshold for the Nth cascade line, $\phi_{N+1}(\omega_{N+1},-\mathbf{k})$, let the pump wave be the (N-1)th cascade $\phi_N(\omega_N,\mathbf{k})$ and the ion acoustic wave be $n_{sN}(\omega_{sN},2\mathbf{k})$. The dispersion relation can be obtained from equations 2.1 and 2.2 by assuming $\omega_{k\theta} \cong \omega_0 \cong \omega_N$ and letting $\omega_{sN} \cong \omega_{sNr} + i\gamma_N$ and $\omega_{N+1} \cong \omega_{k\theta} - \Sigma_{q=1}^{N}\omega_{sqr} + i\gamma_N$:

$$\begin{aligned}&\left[i\omega_0(2\gamma_N + \nu_e) - 2\omega_0\Sigma_{q=1}^{N}\omega_{sqr}\right]\left[-i\omega_{sNr}(2\gamma_N + \nu_i) + \omega_{sNr}^2 - 4k^2C_s^2 - \gamma_N(\gamma_N + \nu_i)\right] \qquad (2.7)\\ &= k_1^2\left[k_0^2 + k_\perp^2\omega_0^2/(\omega_0^2 - \Omega_e^2)\right]\cdot(\omega_p^4 / 4\pi n_0 M\omega_0^2)|\phi_N|^2\end{aligned}$$

The threshold for the Nth cascade line is now obtained by letting $\gamma_N = 0$ and reducing equation 2.7:

$$|\phi_N|_{th}^2 = G_N|\phi|_0^2 = G_N|E_{pth}(k,\theta)|^2 \cos^2\theta / 2\left[k_0^2 + k_\perp^2\omega_0^2 / (\omega_0^2 - \Omega_e^2)\right], \qquad (2.8)$$

where $\Sigma_{q=1}^{N}\omega_{sqr} \cong N\omega_{sNr}$ is assumed; and $G_N = [1 + 16N^2k_1^2C_s^2 / \nu_e(n_e + 2N\nu_i)]\ [\nu_e / (\nu_e + 2N\nu_i)]^{1/2}$.

2.3 Resonant Cascade Process

Similar to the non-resonant case, the threshold field for the resonant decay process is obtained by introducing the instability linear growth rate γ_1 into the wave frequencies and substituting these frequencies into equation 2.3. Letting $\omega_{s1} = 2k_1C_s + i\gamma_1$ and $\omega_1 = \omega_{k\theta} + i\gamma_1$, substitution into equation 2.3 gives the dispersion relation for the resonant decay cascade process [*Kuo and Lee*, 2005]:

$$2k_1C_s\omega_{k\theta}(2\gamma_1+\nu_e)(2\gamma_1+\nu_i)=k_1^2\left[k_0^2+k_\perp^2\omega_{k\theta}^2/\left(\omega_{k\theta}^2-\Omega_e^2\right)\right]\cdot\left(\omega_p^4/\pi n_0 M\omega_{k\theta}^2\right)|\phi|^2. \tag{2.9}$$

Again, the threshold field occurs when $\gamma_1 = 0$, and is obtained from equation 2.9:

$$|\phi|_{th}^2=|\phi|_0^2\cong\left|E_{pth}(k_1,\theta)\right|^2\cos^2\theta/2\left[k_0^2+k_\perp^2\omega_0^2/\left(\omega_0^2-\Omega_e^2\right)\right]. \tag{2.10}$$

Equation 2.10 can be used to calculate the instability threshold field for the resonant cascade process.

A comparison of equations 2.6 and 2.10 shows that the threshold of instability for a resonant cascade process is less than that of a non-resonant cascade process, by a factor of $G_1^{1/2}$. This suggests that the resonant cascade process is more likely to occur than the non-resonant cascade process. If this is indeed the case, then radar observations will observe a decrease in altitude in each step of the cascade. This downward propagation of the Langmuir waves, a characteristic feature of the resonant decay process, occurs because each excited Langmuir wave cannot satisfy the instability dispersion relation at the altitude of excitation. The Langmuir wave therefore propagates downward and parametrically decays.

There is a propagation loss associated with the downward propagation of Langmuir waves from the altitude of excitation to the altitude of decay. Due to collisional and collisionless interactions, the field amplitude of the Langmuir waves will decrease. In order to account for this, the spatial damping rate α is introduced. Existing theory states that the threshold field must be increased by a factor of $e^{\alpha\Delta z}$, where z_0 is the excitation

altitude and z_1 is the decay altitude. The spatial damping rate is derived to be $\alpha \cong \nu_e / 2v_g$, where ν_e is the total effective collision frequency (including Landau damping effect) and $v_g = 3k_{1r}v_{te}^2/\omega_1$ is the Langmuir wave's group velocity. The size of the cascade step, $\Delta z = |z_0 - z_1|$, is found to be:

$$\Delta z = 4\omega_1 k_{1r} C_s L / \omega_p^2(z_0) \tag{2.11}$$

where L is the inhomogeneity scale length L.

Chapter 3

Theoretical Calculations and Discussion

The equations presented in the previous chapter can be evaluated using appropriate values for the conditions in Gakona. Of particular interest are the instability thresholds for the non-resonant and resonant cascade processes. Other calculations will include loss terms associated with each process. Calculated values will be presented and compared with values from previous work in Arecibo, Puerto Rico and Tromso, Norway. Analysis will begin with the statement of the adopted parameters used in the calculations.

3.1 Plasma Parameters

Plasma parameters in the F-region of the ionosphere over Gakona include: HF heater frequency f_0 = 3.3 MHz, electron plasma frequency f_{pe} ~ 4 MHz, electron cyclotron frequency f_{ce} = 1.3 MHz, electron-ion collision frequency ν_{ei} = 500 s^{-1}, ion-neutral particle collision frequency ν_{in} = 0.5 s^{-1}, electron temperature T_e = 2000 K ion temperature T_i = 1000 K, thermal electron velocity $v_{te} = 1.74 \times 10^5$ m/s, thermal ion velocity $v_{ti} = 7.17 \times 10^2$ m/s, sound speed $C_s = 1.6 \times 10^3$ m/s. Note that the ion species in the F-region of the ionosphere is positively ionized atomic oxygen, O^+. The ion mass is taken to be $m(O^+) = M = 16(m_p/m_e)$, where the ratio of the proton mass to electron mass given by m_p/m_e =1836. Also note that in the calculations, angular frequencies are given by $\omega = 2\pi f$.

For the calculations of interest, the parallel and perpendicular components of the pump wave wave number are needed. These values are governed by the parameters of the

detecting radar, MUIR. Due to the fact that the MUIR radar is a backscatter radar, it is necessary to recall that backscatter radars will only detect HFPLs having a wave number equal to twice that of the radar and propagating parallel or antiparallel to the radar. The detectable wave numbers are calculated using the following expressions for Bragg scattering and wave number: $\lambda_0 = \lambda_r / 2$ and $k = 2\pi / \lambda$. For vertical propagation, the parallel and perpendicular components of the pump wave wave number are given by $k_{\|0} = 18.2\ m^{-1}$ and $k_{\perp 0} = 4.75\ m^{-1}$; where $\lambda_{\|0} = \lambda_r / 2\sin\theta_m$, $\lambda_{\perp 0} = \lambda_r / 2\cos\theta_m$, $\theta_m = 75.4°$ is the magnetic dip angle at Gakona, and $\lambda_r = c / f_r$ where c is the speed of light and f_r = 450 MHz.

3.2 Threshold Calculations

3.2.1 Resonant Threshold

A comparison of the non-resonant and resonant cascade process thresholds shows a common factor $|\phi|_0^2$. Since equations 2.6, 2.8, and 2.10 all require this value, it will be the next value considered. Restated here, the threshold condition for the first resonant cascade is given by where $|\phi|_0^2 = (mM/e^2)\{k_1 C_s \omega_{k\theta}^3 \nu_e \nu_i / 2k_1^2[k_0^2 + k_\perp^2 \omega_{k\theta}^2 / (\omega_{k\theta}^2 - \Omega_e^2)]\ \omega_p^2\}$, which can be modified to match the notation and quantities discussed above. Note that $k_0 = k_{\|0}$. The first resonant cascade threshold now takes the form:

$$|\phi|_0^2 = \frac{m_e M}{e^2} \frac{k_1 C_s \omega_{k\theta}^3 \nu_e \nu_i}{2k_1^2 \left(k_{\|0}^2 + k_{\perp 0}^2 \frac{\omega_{k\theta}^2}{\omega_{k\theta}^2 - \omega_{ce}^2} \right) \omega_{pe}^2}, \tag{3.1}$$

where it is recalled that the wave number of the mother Langmuir wave is $k_1 = k_0 + k_\perp$, or $k_1 = k_{\|0} + k_{\perp 0}$; and where the angular frequency $\omega_{k\theta}$ is approximately equal to the frequency of the daughter Langmuir wave since the ion acoustic wave's angular frequency is much smaller in comparison: $\omega_{k\theta} / 2\pi \sim 3.3$ MHz. Before equation 3.1 can

be evaluated, the collision frequencies $\nu_e = \nu_{ei} + \nu_{eL}$ and $\nu_i = \nu_{in} + \nu_{iL}$ are needed. These are obtained by calculating the electron- and ion-Landau damping rates.

The electron-Landau damping rate given in chapter 2 is rewritten as:

$$\nu_{eL} = \left(\frac{\pi}{2}\right)^{1/2} \frac{\omega_0^2 \omega_{pe}^2}{k_{\|0} k_1^2 v_{te}^3} \exp\left(-\frac{\omega_0^2}{2k_{\|0}^2 v_{te}^2}\right); \tag{3.2}$$

where $k_z = k_{\|0}$ for vertical propagation, and k is actually the wave number of the mother Langmuir wave, k_1. Inserting the appropriate values into equation 3.2 yields ν_{eL} = 3.62 Hz leading to ν_e = 504 Hz. In a similar fashion, the ion-Landau damping rate from chapter 2 is rewritten as:

$$\nu_{iL} \cong \left(\frac{\pi}{2}\right)^{1/2} \frac{\omega_s^2}{k_{\|0} v_{ti}} \frac{T_e}{T_i} \exp\left(-\frac{\omega_s^2}{2k_{\|0}^2 v_{ti}^2}\right); \tag{3.3}$$

where ω_s is the angular frequency of the ion acoustic wave, and is taken to be $\omega_s / 2\pi \sim$ 4 MHz. Substitution into equation 3.3 produces ν_{iL} = 19.1 kHz. The total ion collision frequency is now approximated as $\nu_i \approx \nu_{iL}$ since $\nu_{iL} \gg \nu_{in}$.

All the necessary variables in equation 3.1 are now known, thus the resonant cascade threshold field is now calculated. Using the values and results above, this threshold field is found to be $|\phi_{res}|_{th} = \sqrt{(|\phi|_0^2)}$ = 3.53 mV → $|E_{res}|_{th} \sim$ 0.0644 V/m, using $E \propto \nabla\phi = k\phi$.

3.2.2 Non-Resonant Threshold

The threshold for the non-resonant cascade process is given by equation 2.6, $|\phi_1|_{th}^2 = G_1|\phi|_0^2$. In order to obtain a value for equation 2.6, the factor G_1 must first be calculated. Substitution into $G_1 = [1+16k_1^2C_s^2/\nu_e(\nu_e+2\nu_i)]\ [\nu_e/(\nu_e+2\nu_i)]^{1/2}$ leads to G_1 = 127, ultimately leading to $|\phi_{nonres}|_{th} = \sqrt{(|\phi_1|_{th}^2)}$ = 39.8 mV → $|E_{nonres}|_{th} \sim$ 0.726 V/m.

3.2.3 Nth Non-Resonant Threshold

For the excitation of the Nth cascade line of the non-resonant decay process, the threshold is obtained using equation 2.8, $|\phi_N|_{th}^2 = G_N|\phi|_0^2$. The factor G_N is similar to G_1, and is given by:

$$G_N = \left[1+\frac{16N^2k_1^2C_s^2}{\nu_e(\nu_e+2N\nu_i)}\right]\left(\frac{\nu_e}{\nu_e+2N\nu_i}\right)^{1/2}. \tag{3.4}$$

This can be simplified when the ratio of the total ion collision frequency to the total electron collision frequency is considered. Recalling ν_e = 504 Hz and ν_{iL} = 19.7 kHz, the ratio of the collision frequencies is $\nu_i / \nu_e \approx 40$ and it is clear that $2N\nu_i \gg \nu_e$. With this, $16N^2k_1^2C_s^2 / \nu_e(\nu_e + 2N\nu_i) \approx 16N^2k_1^2C_s^2 / 2N\nu_e\nu_I$, and equation 3.4 can be further simplified with $8Nk_1^2C_s^2 / \nu_e\nu_i \gg 1$. Equation 3.4 now becomes

$$G_N \approx 8N^{1/2}\frac{k_1^2C_s^2}{\left(2\nu_e\nu_i^3\right)^{1/2}} = 129N^{1/2}, \tag{3.5}$$

and the threshold for the Nth cascade line in the non-resonant decay process is found to be $|\phi_{N,nonres}|_{th} = \sqrt{(|\phi_N|_{th}^2)} = 40.2\ N^{1/4}$ mV → $|E_{N,nonres}|_{th} \sim 0.732\ N^{1/4}$ V/m.

3.3 Propagation Loss Calculations

Direct comparison of the three threshold values indeed shows that the threshold field for the resonant process is less than the threshold fields for the non-resonant process. The prediction of experimentally observing the resonant process instead of the non-resonant process is hereby justified. Attention is now turned to the calculation of the necessary downward propagation of the Langmuir waves associated with the resonant cascade

process. From the previous chapter, the change in altitude, Δz, is a function of the inhomogeneity scale length of the plasma density, L. For high latitude locations like Gakona, this value is typically 15 km. However, for heating experiments, the plasma density inhomogeneity scale length can increase in size due to the swelling effect discussed in the previous chapter. Although this value wasn't measured, the value at Tromso can be adopted because Gakona and Tromso are at similar high latitudes and the F-region of the ionosphere behaves similarly. Thus, L ~ 25 km is assumed for the evaluation of equation 2.11, $\Delta z = 4\omega_l k_{lr} C_s L / \omega_p^2(z_0)$. Inserting the proper values, the change in altitude is calculated to be: $\Delta z \sim 121$ m, where $k_{lr} = k_l$ and the Langmuir wave angular frequency is taken as $\omega_l \approx \omega_0$, since the angular frequency of the ion acoustic wave is three orders of magnitude smaller. With the change in altitude Δz, only the spatial damping rate α is needed to calculate the quantity $\alpha\Delta z$. The spatial damping rate was derived in chapter 2 as $\alpha \cong \nu_e / 2v_g$, where $v_g = 3k_{lr}v_{te}^2/\omega_l$ is the Langmuir wave's group velocity. For the values at Gakona, $v_g = 1.01\times10^5$ m/s giving $\alpha = 0.0025$ m^{-1} and $\alpha\Delta z \sim 0.302$. Thus, due to the spatial damping encountered from the downward propagation, in the excitation region of the daughter Langmuir wave the spectral amplitude of the daughter Langmuir wave must meet or exceed that of the mother line by a factor of $e^{\alpha\Delta z} \sim 1.35$ for the cascade to continue. Another way for the cascade to continue is if the wave field $\mathbf{E}_p$ of the HF heater wave has a large enough amplitude.

3.4 Comparison with Previous Work

3.4.1 Threshold Calculations

To further investigate the results of the previous calculations, comparisons can be made with the work done by Kuo and Lee in 2005 at Arecibo and Tromso. For the heating experiments conducted at Arecibo, the F-region plasma parameters are: HF heater frequency $f_0 = 5.1$ MHz, electron plasma frequency $f_{pe} \sim 4$ MHz, electron cyclotron frequency $f_{ce} = 1.06$ MHz, total electron collision frequency $\nu_e = 500$ s^{-1}, ion-neutral

particle collision frequency $\nu_{in} = 0.5\ s^{-1}$, electron and ion temperatures $T_e = T_i = 1000$ K, thermal electron velocity $v_{te} \sim 1.23\times10^5$ m/s, thermal ion velocity $v_{ti} = 7.17\times10^2$ m/s, sound speed $C_s = 1.43\times10^3$ m/s. For a magnetic dip angle of $\theta_m = 50°$ and for vertical propagation of the 430 MHz radar, the parallel and perpendicular components of the pump wave wave number are calculated to be $k_{\|0} = 13.8\ m^{-1}$ and $k_{\perp0} = 11.6\ m^{-1}$. Notice that the total electron collision frequency is provided, not the electron-ion collision frequency. This is because the total electron collision frequency is the sum of the electron-ion collision frequency and the electron-Landau damping rate. At Arecibo, the electron-Landau rate is very small ($\ll 1$ Hz) and is therefore neglected. The ion-Landau damping rate is calculated to be $\nu_{iL} = 3.18$ kHz.

At Tromso, the plasma parameters are: HF heater frequencies $f_0 = 5.423$ and 6.77 MHz, plasma frequency $f_{pe} \sim 4$ MHz, electron cyclotron frequency fce = 1.35 MHz, total electron collision frequency $\nu_e = 10^3\ s^{-1}, \nu_e = 10^3\ s^{-1}$, electron temperature $T_e = 2000$ K, ion temperature $T_i = 1000$ K, thermal electron velocity $v_{te} \sim 1.74\times10^5$ m/s, thermal ion velocity $v_{ti} \sim 7.17\times10^2$ m/s, sound speed $C_s = 1.6\times10^3$ m/s. For a magnetic dip angle of $\theta_m = 78°$, the parallel and perpendicular components of the pump wave wave number corresponding to 933 MHz radar signals are $k_{\|0} = 38.2\ m^{-1}$ and $k_{\perp0} = 8.13\ m^{-1}$. For the 224 MHz radar signals, the wave number components are $k_{\|0} = 9.18\ m^{-1}$ and $k_{\perp0} = 1.95\ m^{-1}$. The ion-Landau damping rates are calculated to be $\nu_{iL} = 37.9$ kHz for the 933 MHz radar and $\nu_{iL} = 0.163$ kHz for the 224 MHz radar.

With these values, the instability threshold fields can be calculated. From equation 3.1, the resonant threshold at Arecibo is $|E_{res}|_{th} \sim 0.0183$ V/m. At Tromso, the resonant threshold fields are $|E_{res}|_{th} \sim 0.0912$ V/m for the 933 MHz radar and $|E_{res}|_{th} \sim 0.0222$ V/m for the 224 MHz radar. Moving on to equation 2.6, the threshold for the first line in the non-resonant process is $|E_{nonres}|_{th} \sim 0.747$ V/m at Arecibo and $|E_{nonres}|_{th} \sim 1.04$ V/m and $|E_{nonres}|_{th} \sim 0.704$ V/m at Tromso, for the 933 and 224 MHz radars, respectively. Finally, from equation 2.8 the thresholds for the Nth cascade line in the non-resonant process are: $|E_{N,nonres}|_{th} \sim 0.701\ N^{1/4}$ V/m for Arecibo, and $|E_{N,nonres}|_{th} \sim 1.05\ N^{1/4}$ V/m and $|E_{N,nonres}|_{th} \sim 2.01\ N^{1/4}$ V/m for the radars at Tromso. The results of

these calculations are summarized in table 3-1, accompanied by the results from the calculations for heating experiments at Gakona for comparative purposes.

Table 3-1: Results from instability threshold calculations for Arecibo, Tromso, and Gakona.

Location	f_0 [MHz]	f_{radar} [MHz]	$\|E_{res}\|_{th}$ [V/m]	$\|E_{nonres}\|_{th}$ [V/m]	$\|E_{N,nonres}\|_{th}$ [V/m]
Arecibo	5.1	430	0.0183	0.747	$.701N^{1/4}$
Tromso	5.432	933	0.0912	1.04	$1.02N^{1/4}$
Tromso	6.77	933	0.0912	1.04	$1.02N^{1/4}$
Tromso	5.432	224	0.0222	0.704	$2.01N^{1/4}$
Tromso	6.77	224	0.0222	0.704	$2.01N^{1/4}$
Gakona	3.3	450	0.0644	0.726	$0.732N^{1/4}$

Analysis of table 3-1 shows that the threshold values for the resonant decay process are less than those for the non-resonant decay process. This comparison supports the theory presented in chapter 2 and extends Kuo and Lee's 2005 theory at Arecibo and Tromso to Gakona. Because the resonant process is believed to be the method at which the HFPLs will cascade, experiments will be performed to look for decreases in altitude for each step of the cascade, the characteristic feature of a resonant cascade process. The remaining calculations in this chapter will focus on the change in altitude of each step in the resonant cascade. Another trend to note about the data presented in table 3-1 is that the values for Gakona are similar to those for Tromso when they are compared to the values for Arecibo. This was expected because both Gakona and Tromso are high latitude locations, with similar parameters.

3.4.2 Propagation Loss Calculations

As mentioned above, the inhomogeneity scale length of plasma density for Tromso is L ~ 25 km. At Arecibo, L ~ 50 km is assumed. With these values, the change in altitude that results from the downward propagation of Langmuir waves in the resonant cascade can be calculated using equation 2.11. Also, the group velocity of the Langmuir wave v_g, the spatial damping rate α, and the factors $\alpha\Delta z$ and $e^{\alpha\Delta z}$ can be calculated. For Arecibo, the following values are obtained: $\Delta z = 360$ m, $\alpha\Delta z \sim 2.56$, and $e^{\alpha\Delta z} \sim 12.9$. For the

933 MHz radar at Tromso: Δz = 400 and 499 m, $\alpha\Delta z \sim 1.62$ and 2.52, and $e^{\alpha\Delta z} \sim 5.07$ and 12.5 for f_0 = 5.432 and 6.77 MHz, respectively. For the 224 MHz radar at Tromso: Δz = 96.2 and 119 m, $\alpha\Delta z \sim 1.62$ and 2.52, and $e^{\alpha\Delta z} \sim 12.5$ and 1.35 for f_0 = 5.432 and 6.77 MHz, respectively. These calculations are summarized in table 3-2, and once again the data from Gakona is included for comparative purposes.

Table 3-2: Results from altitude loss calculations for Arecibo, Tromso, and Gakona.

Location	f_0 [MHz]	f_{radar} [MHz]	L [km]	Δz [m]	$\alpha\Delta z$	$e^{\alpha\Delta z}$
Arecibo	5.1	930	50	368	2.56	12.9
Tromso	5.432	933	25	400	1.62	5.07
Tromso	6.77	933	25	499	2.52	12.5
Tromso	5.432	224	25	96.2	1.62	5.07
Tromso	6.77	224	25	119	2.52	12.5
Gakona	3.3	950	25	121	0.302	1.35

Examination of table 3-2 provides the expected change in altitude for each resonant cascade step observed in the Langmuir sideband excited by PDI.

Chapter 4

Experimental Data and Discussion

Two HF space plasma heating experimental campaigns were conducted to support the theory behind the parametric decay instability (PDI) presented in this thesis. The first campaign was conducted on March 18, 2006 from 03:00 – 05:00 (UT), the second on August 9, 2006 from 03:00 – 04:00 (UT). These heating experiments were performed at the NSF/DoD High Frequency Active Auroral Research Program (HAARP) facility in Gakona, Alaska. Data were recorded via incoherent scatter radar (ISR) observations from the 450 MHz Modulated UHF Ionosphere Radar (MUIR) onsite at HAARP. It is important to note that the HFPLs have an angular distribution around the earth's geomagnetic field, but the radar will only detect those that propagate parallel or antiparallel to the propagation direction of the radar. Other diagnostic tools at HAARP included an ionosonde, a mangnetometer, a VHF classic riometer, and a VLF receiving system. The ionosonde played the most important role in monitoring the ionospheric conditions, as it was used to measure peak plasma frequency and to track absorption.

An additional set of data is provided at the end of this chapter to support the proposed theory. This data was taken on February 3, 2005 at the HAARP facility [courtesy of Professor Brenton Watkins of the University of Alaska Fairbanks (UAF)]. It is important to note that at the time the 2005 experiments were conducted, the construction of MUIR had not been completed. The radar used to collect the set of data from the February 2005 campaign was the Advanced Modular Incoherent Scatter Radar (AMISR). Since the construction of MUIR, AMISR has been upgraded and its duties assigned to MUIR.

4.1 March 2006 Campaign

For the experiments conducted in March 2006, the HF heater and radar were tilted off-zenith by 7.5° and the azimuth was set to 24°. The heater operated in full-power O-mode with CW polarization, and its frequency ranged from 2.76 – 4.3 MHz. Specifically, frequencies f_0 = 2.76, 3.3, 4.2, 4.3 MHz were used to excite the PDI. The coded-long-pulse technique was employed to detect the HFPLs in the frequency range of 3.8 – 4.8 MHz and altitude range of 150 – 300 km. The power spectra density of the HFPLs were returned in a 998-by-1000 frequency/altitude array, with bin sizes of 1 kHz and 150 m. Five plasma measurements were made 03:00 – 05:00 (UT), of the following durations: 22, 13, 39, 1.2, and 23 minutes. For all the experiments except one, the heater operated in a pulsed mode of 1 minute on, 1 minute off. For the experiment without pulsed operation, the heater remained on for the duration of the experiment.

Of the five experiments conducted in this campaign, only one observed the PDI. The other four did not show any HFPLs from PDI, only low intensity HFPLs around the heater frequency were observed. Absorption was high during the time these experiments were conducted, and it is believed that this anomalous absorption caused by proton precipitation is the reason PDI events were not excited. (See Appendix A for a discussion of absorption.) For Gakona, proton precipitation at high altitudes is not uncommon. For the case where PDI was observed, three distinct HFPLs were witnessed at 4.296 MHz, 4.288 MHz, and 4.280 MHz, near the altitude of 213 km. Decreasing in intensity, the three HFPLs represent the mother Langmuir pump wave generated by PDI and two cascade daughter Langmuir waves parametrically excited. The observed PDI event and subsequent cascade is believed to arise via the resonant cascade process. Figure 4-1 below plots the power spectra density as a function of range and frequency. The three discussed HFPLs are easily seen, and it is noted that these HFPLs are down-going, frequency upshifted Langmuir waves. A two-dimensional slice of the figure 4-1 can be used to show the three HFPLs at a fixed altitude. This is provided in figure 4-2, for a fixed altitude of 212.8 km.

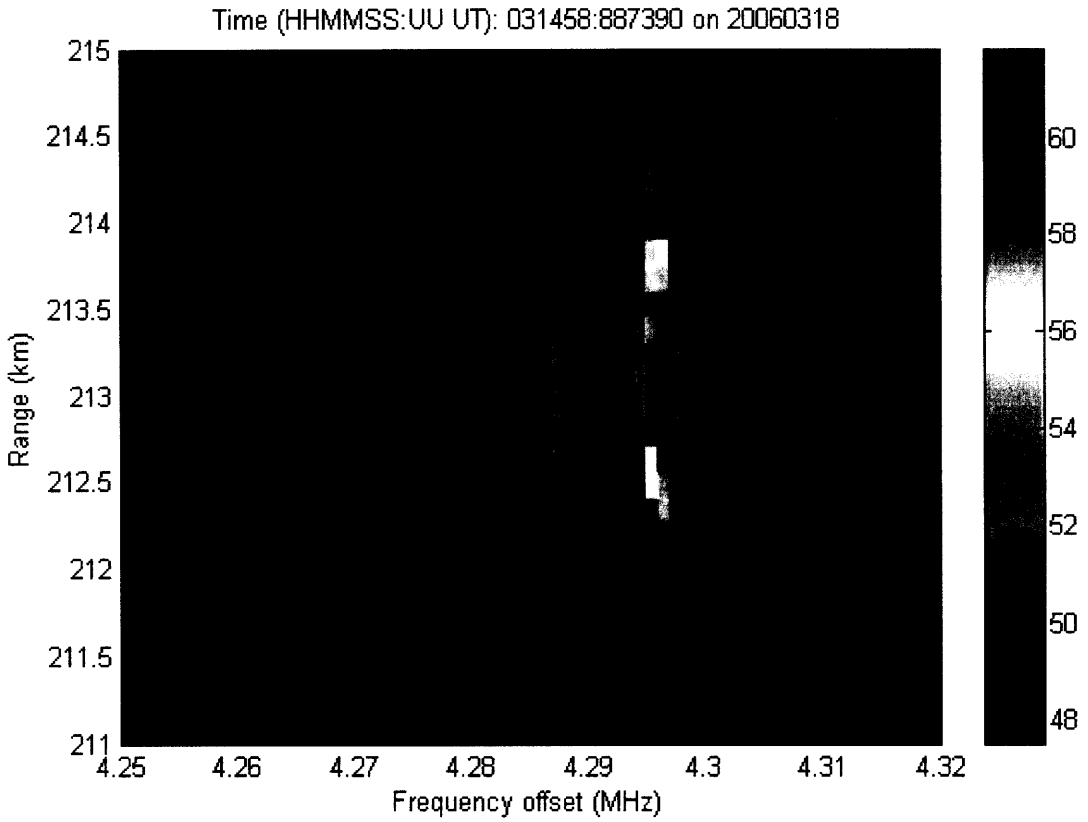

Figure 4-1: Plot of power spectra density of PDI event observed on March 14, 2006 at 03:14:58 (UT). The three observed HFPLs correspond to frequencies of 4.296, 4.288, and 4.280 MHz in order of decreasing intensity.

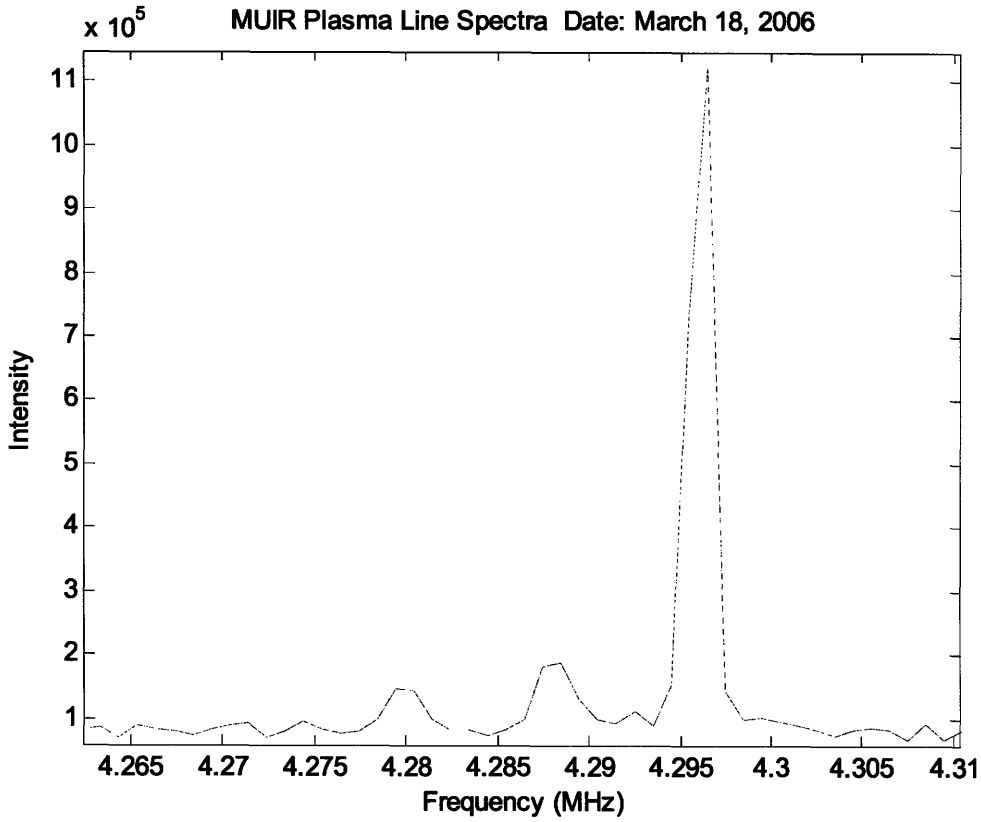

Figure 4-2: Intensity versus frequency for a fixed altitude of 212.8 km from PDI event observed on March 14, 2006 at 03:14:58 (UT). As in figure 4-1, the three observed HFPLs correspond to frequencies of 4.296, 4.288, and 4.280 MHz in order of decreasing intensity.

In order to support the claim that the PDI event and cascade shown in figure 4-1 were in fact caused by the resonant decay process, the altitudes of the three HFPLs need to be obtained. With the height of each HFPL, the change in altitude of each cascade step, Δz, can be calculated and compared with the theoretical values. Despite its straightforwardness, this task proved to be impossible to accomplish given the way the data were recorded. As previously mentioned, the power spectra density is given as a function of range and frequency. Fixing frequency and plotting power spectra density versus range does not yield the desired quantity, nor does plotting power spectra density versus frequency for a fixed range value. The ability to plot the signal-to-noise ratio as a function of range and time and the power density spectra as a function of intensity and time would allow for complete analysis. For future campaigns, it is proposed that a new

data acquisition technique be employed to record the data as a function of time, thereby gaining the ability to capture the sought after quantities.

4.2 August 2006 Campaign

The experiments performed during the summer campaign conducted in August 2006 were different than those conducted in March 2006. With the azimuth set to 204° and the zenith set to 15°, the HF heater and radar were tilted along the earth's magnetic field lines. Such geometry was chosen because parallel propagation maximized the chances of exciting PDI events. The heater was set to operate pulsed O-mode of CW polarization at a power level of 940 kW and frequency f_0 of 3.3 MHz. The pulsing was a 10-second cycle, where the heater was on for 2 seconds and off for the remaining 8 seconds. Unlike the spring experiments, an uncoded-long-pulse technique was used to detect the HFPLs. The uncoded long pulse was characterized by a 998 μs pulse length and a 10 ms IPP. Experiments ran for approximately forty minutes, generating approximately two-minute sets of data. A typical range-time-intensity plot is given in figure 4-3, illustrating the 10-second cycle of the heater.

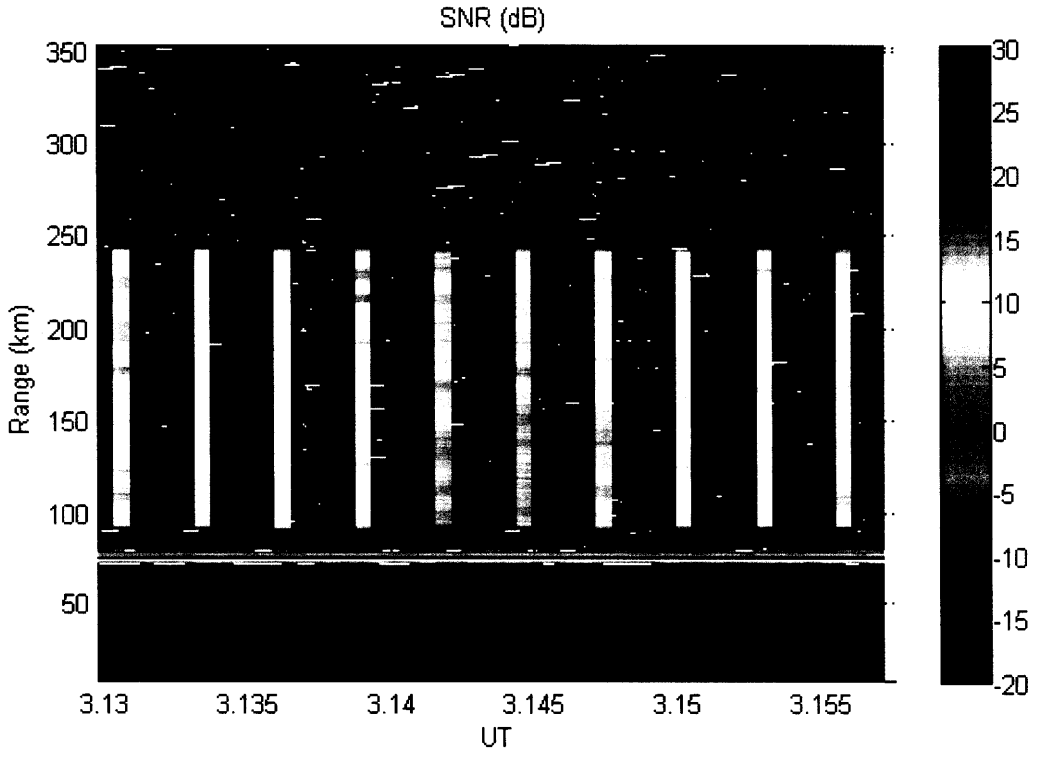

Figure 4-3: Range-time-intensity plot of nine full pulsed heater cycles for typical case on August 9, 2006. Each heater cycle is 10 seconds long, where the heater on for the first 2 seconds and off for the last 8 seconds. Note that the intensity is the value of the signal-to-noise ratio received by the MUIR radar.

Nearly all of the data sets from the beginning of the experimental time period show evidence of PDI excited cascades. The excitation of PDI cascades follows the heater pulse-cycle, that is, cascades are observed for two seconds when the heater is on. When the heater is off, no HFPLs are observed and only background noise is present. The plot in figure 4-4 shows the power spectra density versus frequency, and illustrates cascade of HFPLs. Note that this plot corresponds to the two-second interval of heating. The noise level, obtained from plotting the power spectra density versus frequency during a time interval where the heater is off, is ~ 6 x 10^3 (three orders of magnitude less than the intensity of the HFPLs). For time periods where the heater is off, only a noisy signal of this size is observed. Towards the end of the experiments and even after experiments were completed, absorption increased and very few PDI events were observed. As in the case of the March 2006 experiments, the anomalous absorption is believed to be caused by proton precipitation.

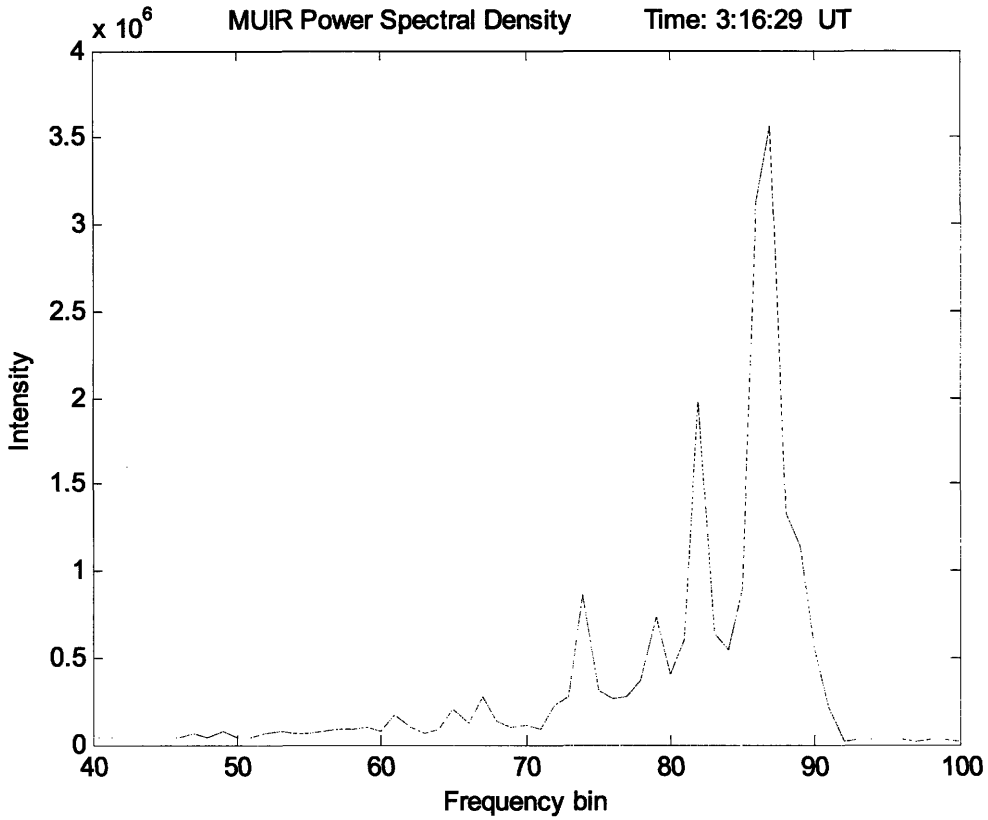

Figure 4-4: Power spectra density versus frequency during heating from PDI event observed on August 9, 2006 at 03:16:29 (UT). Observed behavior is common throughout heating experiments. When the heater is off a similar plot would show no cascading HFPLs, it would only show a noise level of ~6 x 10^3 .

Similar to the case in the experiments in March, positive identification of a resonant cascade process over a non-resonant cascade process cannot be made. Furthermore, because an uncoded long pulse technique was used, the quality of data is poor compared to the data from March. Although very little can be quantitatively extracted from the data, the excitation of PDI is qualitatively identified, as clearly shown in figure 4-4.

4.3 February 2005 Campaign

Because the data from the two experimental campaigns in 2006 failed to provide certainty in the diagnosis of the cascade type witnessed at Gakona, additional data is examined. This additional data comes from earlier experiments conducted in 2005, as discussed above [courtesy of Professor Watkins at UAF]. The experimental conditions for this campaign were similar to the ones described for the August 9, 2006 campaign. AMISR was used to record the data, and figure 4-5 below qualitatively shows the frequency spectra of the observed HFPLs, where f_0 represents the frequency of the HF heater waves.

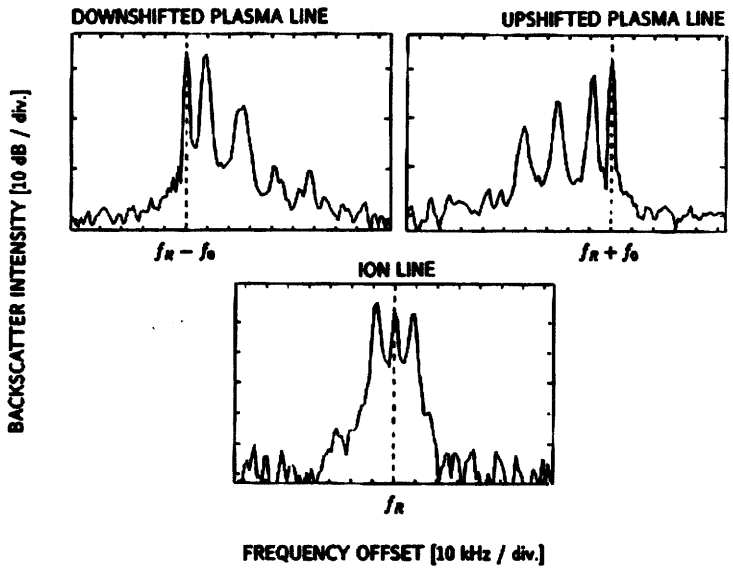

Figure 4-5: Backscatter intensity of received signal from AMISR. Shown here are the frequency spectra of detected waves. The two plots on top show the downshifted and upshifted plasma lines, respectively, and the bottom plot shows the ion line [*Watkins*, 2005].

Cascading Langmuir waves are clearly identified in plots of upshifted and downshifted plasma lines. Note that the downshifted plasma line corresponds to up-going Langmuir waves detected by AMISR and the upshifted plasma line corresponds to down-going Langmuir waves. Recall that upshifted plasma lines were presented in figures 4-1, 4-2, and 4-4. Three peaks are seen in the plot of the ion line. The two outer peaks correspond

to the ion acoustic waves excited with the downshifted and upshifted plasma lines. The central peak corresponds to a purely growing mode.

Presented in figure 4-6 is a data set from the 2005 campaign. The top plot of signal- to-noise ratio as a function of range and time shows detected HFPLs in an altitude range of approximately 150 – 325 km. The poor range resolution is noted: individual HFPLs cannot be identified. In the early stages of AMISR, range resolution was on the order of 300 km, as illustrated by the top plot in figure 4-6. The range resolution will be discussed later in this chapter. The bottom plot in figure 4-6 of power spectra density as a function of frequency offset and time shows the frequency spectra of detected HFPLs. Multiple steps of frequency upshifted Langmuir waves are present in the cascade.

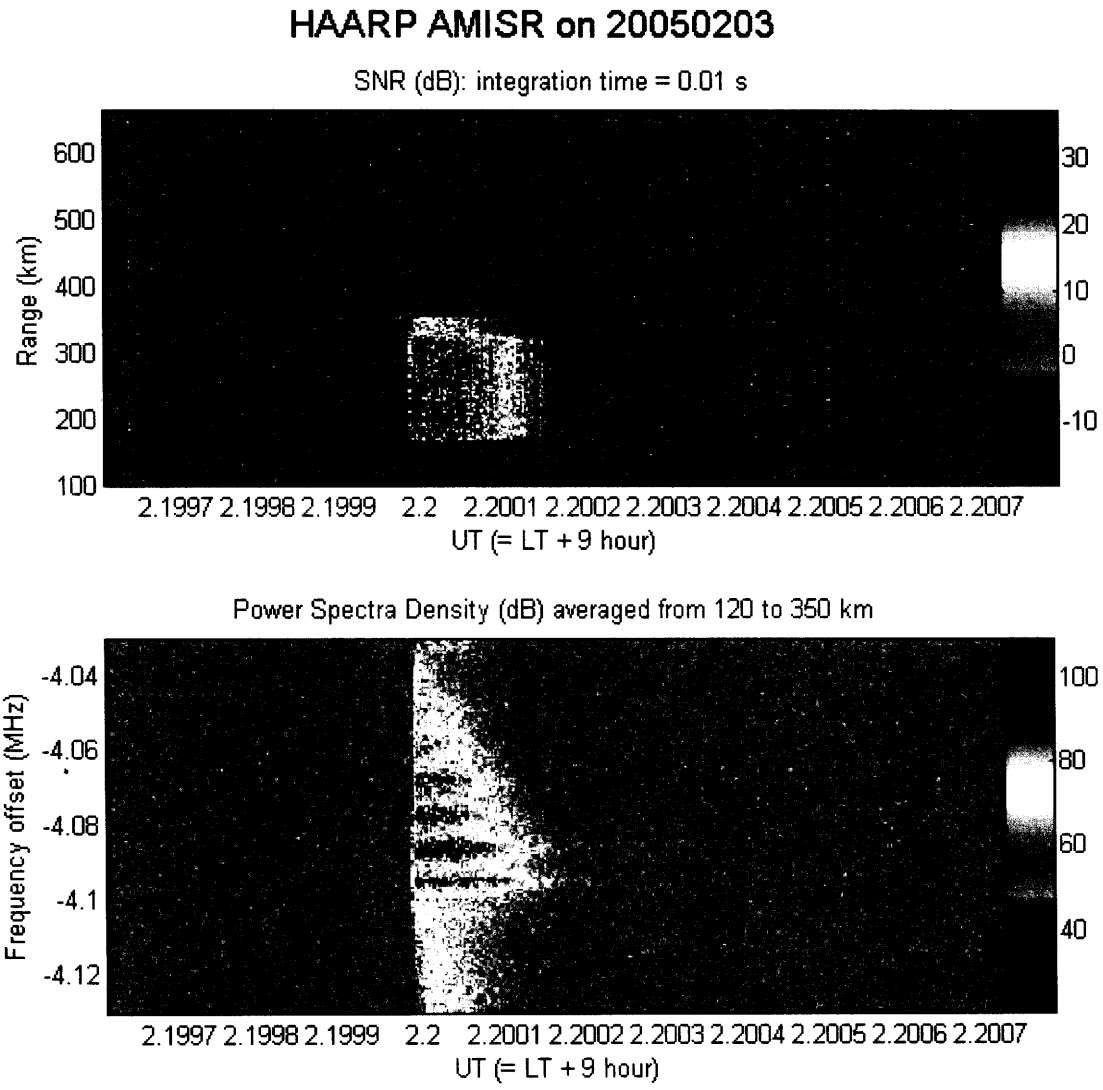

Figure 4-6: AMISR data from February 3, 2005. The top figure of signal-to-noise ratio versus range and time shows HFPLs in a range of 150 – 325 km. The bottom figure of power spectra density versus frequency and time shows multiple HFPL cascade steps over a frequency offset range of 4.05 – 4.10 MHz [*Watkins*, 2005].

What makes this data set special is the manner in which it is presented. The ability to see both the signal-to-noise ratio/range and the power spectra density/frequency offset allows the resonant process to be confidently identified as method by which the HFPLs cascade. Although the decay altitudes of each HFPL cannot be extracted from the data set plotted in figure 4-6, they are not needed for accurate, qualitative identification of the resonant cascade process. While the data itself is not enough to identify the resonant

process over the non-resonant process, when coupled with the notion that the resonant cascade process has a lower instability threshold and therefore predicted to excite PDI events before the non-resonant process, this data completes the picture. Despite the poor range resolution of AMISR in its early stages of operation, the fact that HFPLs are present over a broad range of altitudes along with the fact that the resonant cascade process is expected due to its lower threshold is reason enough to classify the observed cascade as the result of a resonant decay process.

Chapter 5

Conclusion

Established theory by Kuo and Lee suggests that the resonant cascade process has a lower instability threshold than the non-resonant cascade process, and therefore PDI excited HFPLs in the Langmuir sideband will resonantly cascade. If such theory is true, then incoherent scatter radar observations will show characteristic behavior of the resonant cascade process where each Langmuir wave in the cascade series will propagate downward from its excitation height to its decay height. Measurements of the field strengths and of altitudes of the observed cascade steps are ways to support this theory.

To test the theory for a new location, the instability thresholds were calculated using the physical parameters at Gakona. In order to calculate the fields, both the electron- and ion-Landau damping rates were needed. The calculations proved that Landau damping plays a more important role for ions than it does electrons. In fact, it can be said that electrons are primarily affected by collisional damping, with collisionless damping playing only a minor role. The opposite is true for ions, where collisionless damping far exceeds the collisional damping. Moving on to the values for the instability thresholds, calculations confirmed the hypothesis that the resonant cascade process has a smaller threshold than the non-resonant cascade process.

The calculated thresholds for Gakona were compared with values from Arecibo and Tromso from previous experiments. An important similarity between Gakona and Tromso is geographic latitude. Many plasma parameters for the two locations were comparable, including magnetic dip angle, plasma and electron cyclotron frequencies, electron and ion temperatures, electron and ion thermal velocities, sound speed, and inhomogeneity scale length of plasma density. Given the number of similarities, it comes as no surprise that the calculated values for instability thresholds are similar in their

comparison with the values from Arecibo. With positive results from the extension of existing theory to Gakona, the next step was to seek agreement between theory and HF heating experiments, where the source mechanism for producing cascading HFPLs will be the resonant process.

Results from HF heating experiments conducted at the HAARP facility in Gakona in March and August, 2006 showed the presence of PDI excited Langmuir waves in incoherent backscatter radar observations. These HFPLs were frequency upshifted plasma lines detected by MUIR. Unfortunately, no evidence to positively identify the source mechanism of the cascade was manifested from analysis of data. This was true for both of the 2006 campaigns. The problem was in the way data were recorded. For a complete and thorough analysis, more data was needed. A data set from a previous campaign at Gakona provided the needed connection of theory and experiment. This data, collected in February 2005, is beneficial to this thesis because it provides what the data from 2006 could not. The resonant process was identified as the source mechanism for the observed cascade of HFPLs through analysis of the altitude and frequency spectra of HFPLs. Even though the data is of poor quality in terms of altitude resolution, the fact that HFPLs were detected over a broad range of 175 km shows that HFPLs are present at other places than just the initial excitation altitude. When this observation is coupled with the theory behind the resonant cascade process, such as downward propagation from excitation altitude to decay altitude, it can be concluded that the HFPLs are propagating downward from their excitation height to a lower-altitude decay height and also that subsequent cascade steps repeat this behavior. Only now can the pieces of evidence be combined to qualitatively identify the resonant process and simultaneously rule out the non-resonant process. Neither the theory nor the evidence individually possess the ability to positively identify the resonant process; they can only observe characteristics of the resonant process. Their combination completes the analyses of the PDI and the source mechanism of cascading HFPLs caused by the PDI.

Appendix A

Comments on Absorption

Absorption has been said to create unfavorable conditions for the excitation of PDI events. When proton precipitation occurs, additional electrons are created in the ionospheric plasma to cause anomalous absorption of HF heater waves and as a result no PDI events are observed. The ability to identify absorption in near real-time is important when conducting heating experiments, allowing one to accurately identify a mechanism that might prevent the excitation of PDI events. Examination of an ionogram provides the simplest way to check the level of anomalous absorption. With this in mind, the ionosonde at HAARP was set to record ionograms every five minutes. During normal conditions, ionograms show clear backscatter traces of O-mode and X-mode waves; however during periods of increased proton precipitation the ionogram will show little to no traces, corresponding to little to no plasma. The following two figures provide a comparison between the aforementioned cases of normal plasma conditions and increased absorption.

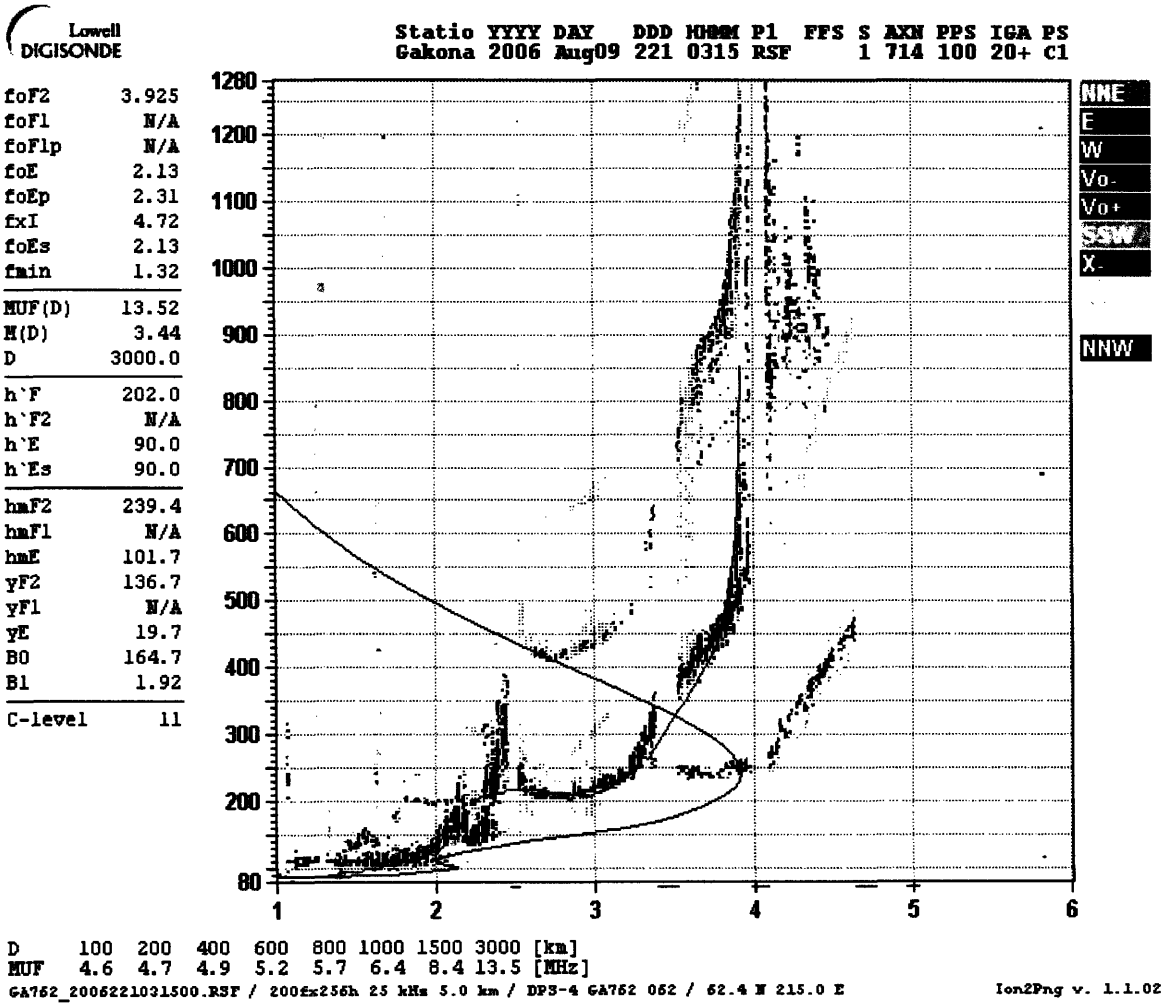

Figure A-1: Ionogram from the HAARP DPS-4 System #039 Digisonde, taken on August 9, 2006 at 03:15 (UT). Note the clear trace of the F-region of the ionosphere. This ionogram represents a typical case where there is little to no absorption.

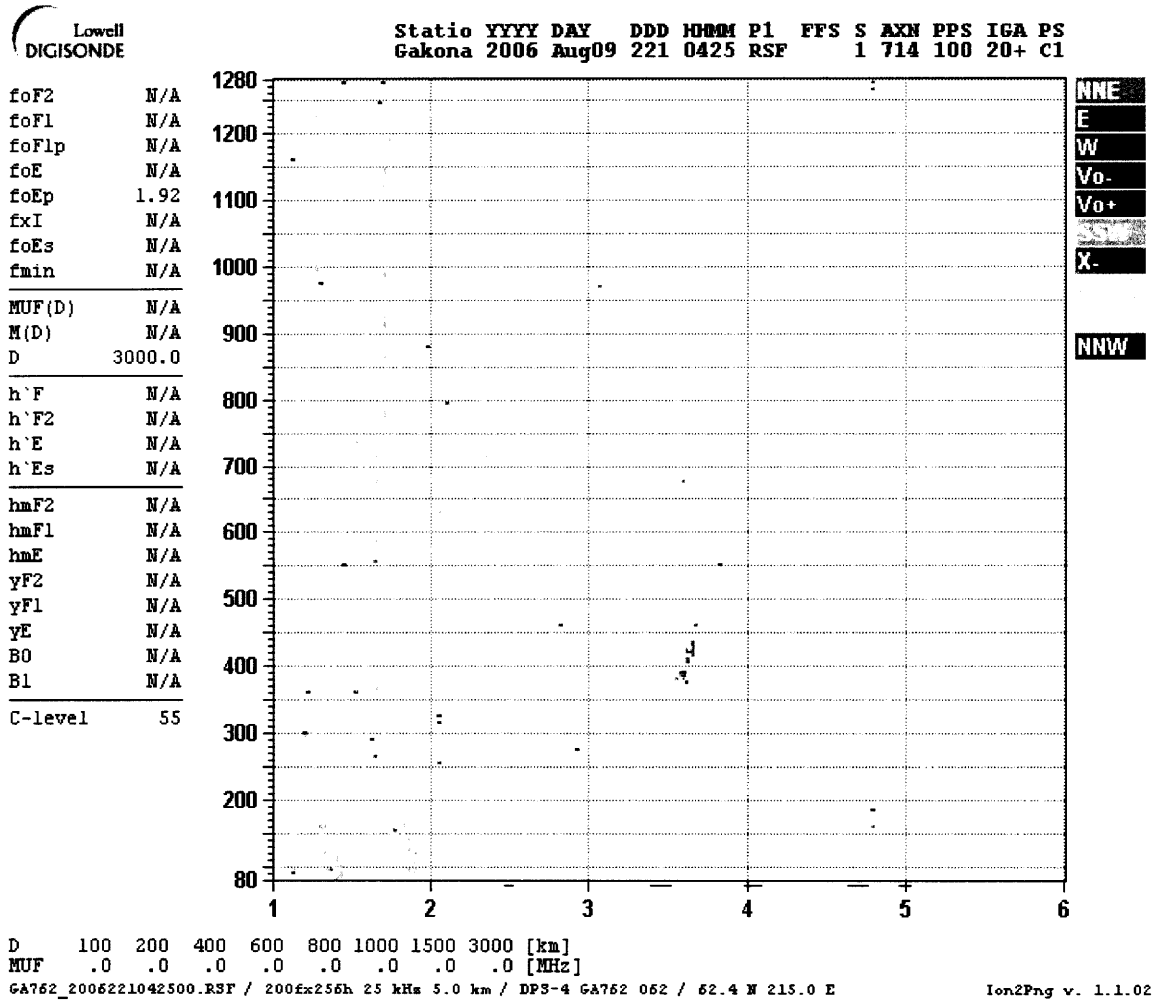

Figure A-2: Ionogram from the HAARP DPS-4 System #039 Digisonde, taken on August 9, 2006 at 04:25 (UT). Note the absence of the trace of the F-region. This ionogram represents a typical case where there is a high level of absorption.

Bibliography

[*Kuo and Lee*, 2005]: Kuo, S. P. and Lee, M. C., Cascade spectrum of HF enhanced plasma lines generated in HF heating experiments, J. *Geophys. Res.*, *110*, A01309 (2005).

[*Lee et al.*, 1997]: Lee, M.C., R.J. Riddolls, K.D. Vilece, N.E. Dalrymple, M.J. Rowlands, D.T. Moriarty, K.M. Groves, M.P. Sulzer, and S.P. Kuo, Laboratory reproduction of Arecibo experimental results: HF wave enhanced Langmuir waves, *Geophys. Res. Lett.*, *24*, 115 (1997).

[*Lee et al.*, 2006]: Lee, M.C., Rezy P., W.J. Burke, A. Labno, L.M. Burton, J.A. Cohen, S.E. Dorfman, A.J. Coster, M.P. Sulzer, and S.P. Kuo, Did Tsunami-launched Gravity Waves Trigger Ionospheric Turbulence over Arecibo?, *J. Geophys. Res.* (2006)

[*Pradipta*, 2006]: Pradipta, R., Personal communication, Massachusetts Institute of Technology (2006).

[*Watkins*, 2005]: Watkins, B., Personal communication, University of Alaska Fairbanks (2005).